Received: 14 September 2019 | Revised: 28 October 2019 | Accepted: 29 November 2019

DOI: 10.1002/asl.949

RESEARCH ARTICLE

Atmospheric Science Letters RMetS

Formation of a kind of heavy-precipitation-producing mesoscale vortex around the Sichuan Basin: An along-track vorticity budget analysis

Shuang-Lei Feng[1,2] | **Shuang-Long Jin**[1,2] | **Shen-Ming Fu**[3] | **Jian-Hua Sun**[4] | **Yuan-Chun Zhang**[4]

[1]State Key Laboratory of Operation and Control of Renewable Energy & Storage Systems, China Electric Power Research Institute, Beijing, China

[2]Electric Power Meteorology State Grid Corporation Joint Laboratory (CEPRI), Beijing, China

[3]International Center for Climate and Environment Sciences, Institute of Atmospheric Physics, Chinese Academy of Sciences, Beijing, China

[4]Laboratory of Cloud–Precipitation Physics and Severe Storms, Institute of Atmospheric Physics, Chinese Academy of Sciences, Beijing, China

Correspondence
Shen-Ming Fu, International Center for Climate and Environment Sciences, Institute of Atmospheric Physics, Chinese Academy of Sciences, Beijing 100029, China.
Email: fusm@mail.iap.ac.cn

Funding information
National Key R&D Program of China, Grant/Award Number: 2018YFC0809400

Abstract

This study investigates the formation of a type of mesoscale vortex around the Sichuan Basin (i.e., the southwest vortex [SWV]) that usually induces heavy precipitation, based on a semi-idealized simulation of eight similar SWV-formation events. After producing a reasonable SWV that shares salient features with the events used in composite, a trajectory analysis is conducted and an along-track vorticity budget is constructed. The results show that approximately 64.7% of the air particles related to SWV formation originate from four source regions outside the vortex. The largest contribution of cyclonic vorticity associated with the SWV formation (approximately 67.7%) comes from the lower levels southwest of the vortex and is due mainly to tilting. The second-largest contribution (approximately 19.4%) is made by air particles that originate from the upper levels south of the SWV and is also due mainly to tilting. By contrast, for the other two sources (the upper levels west and southwest of the vortex), the convergence-related horizontal shrinking generally dominates their cyclonic-vorticity production. Overall, along the tracks of the air particles, vertical motions and water-vapor phase transitions affect the vorticity variation significantly via modulating divergence-related vorticity production/dissipation (i.e., the stretching effect), and this is vital for the SWV formation.

1 | INTRODUCTION

A southwest vortex (SWV) is a unique type of mesoscale vortex that forms around the Sichuan Basin (SCB) east of the Tibetan Plateau (TP) (Lu, 1986; Zhao and Fu, 2007; Fu *et al*., 2015). This type of vortex frequently induces torrential precipitation that results in severe flood events over the Yangtze River Valley (Zhao *et al*., 2004) and both Northern (Lu, 1986) and Southern China (Fu *et al*., 2011, 2014). For decades, much effort has gone into understanding the SWVs and their associated precipitation. Related studies can be divided roughly into four interconnected groups: (a) climatological and statistical analyses that mainly reveal SWV spatiotemporal characteristics, source region and tracks (e.g., Chen *et al*., 2003; Zhong *et al*., 2014); (b) classification and composite analyses that divide SWVs into different types and reveal the key features of each type as well as the main differences and similarities among the different types (e.g., Fu *et al*., 2015; Zhang *et al*., 2015); (c) observational and modelling studies of the precipitation

and convective activities associated with SWVs (e.g., Kuo *et al*., 1988; Ni *et al*., 2017); and (d) diagnostic studies of the mechanisms governing SWV formation, evolution and displacement (e.g., Zhao and Hu, 1992; Wang and Tan, 2014).

In group (d), many studies have investigated the vorticity variation associated with SWVs to understand their formation/evolution. For instance, Zhao and Hu (1992) calculated the vorticity budget of a heavy-rainfall-producing SWV in the summer of 1981 and found that friction and latent heating both contributed to lower-level convergence around the SCB, which was vital for SWV formation. Wang and Tan (2014) produced an idealized SWV using a dry dynamic idealized simulation. Their vorticity-budget results indicate that the SCB played a secondary role in generating that SWV, with the TP and Hengduan Cordillera being more important. Fu *et al*. (2015) calculated the vorticity budgets of the SWVs in 14 consecutive summers. They proposed the main similarities among those SWVs to be that the convergence-related horizontal shrinking and vertical transport of cyclonic vorticity dominated their formation/development whereas the horizontal transport and tilting acted mainly in an opposite manner. Li *et al*. (2017) investigated the effects of the moving-off Tibetan plateau vortices on the genesis of SWVs. They found that the moving-off plateau vortices could contribute to the SWVs' formation via strengthening cyclonic vorticity, convergence and ascending motion.

However, although vorticity analyses/budgets have been widely used in studies of SWV formation, two questions remain unanswered: where do the air particles (that form the SWV) with strong cyclonic vorticity come from, and which factors control their vorticity variation? Therefore, the primary purpose of the present study was to answer these two scientific questions. As documented in previous studies, SWVs can form under many different conditions (Lu, 1986; Zhao *et al*., 2004). In the present study, we focus mainly on SWVs that are initiated under the influences of the eastward-propagating convective systems that originate over the TP. This is because SWVs that form in this way usually have stronger intensity and cause heavier precipitation (Lu, 1986; Zhang *et al*., 2015; Li *et al*., 2017).

The reminder of this paper is structured as follows. The data, model setup and methods are presented in Section 2, the main results are given in Sections 3 and 4 and conclusions are drawn in Section 5.

2 | DATA, MODEL AND METHODS

2.1 | Data and model information

To show the common features of SWVs that form under the influences of the eastward-propagating convective systems that originate over the TP, we conduct a semi-idealized simulation based on a composite of typical SWVs in the summer of 2016 (Fu *et al*., 2019). One of the most remarkable characteristics among these eight events is that an SWV forms during the moving-out stage of a strong convective system that is generated over the TP. In addition, in all eight events, the SWV formation is closely related to a strong low-level southwesterly wind south of the vortex, with a half of them qualifying the standard of a low-level jet (not shown). The six-hourly 0.5° × 0.5° Climate Forecast System data (Saha *et al*., Saha, 2010) is used (a) to generate the initial and boundary conditions for the semi-idealized simulation and (b) for simulation validation. The rain-gauge-based precipitation data from the China Meteorological Administration are used to evaluate the precipitation simulation.

The model configuration and simulation design are the same as those used by Fu *et al*. (2019): they use a one-way triple-nested (36, 12 and 4 km) convection-permitting version of the Weather Research and Forecasting (WRF) model (Skamarock *et al*., Skamarock *et al*., 2008) that consists of 331 × 241 (d01), 541 × 331 (d02) and 1,141 × 721 (d03) grid points (not shown). The WRF single-moment six-class microphysics scheme (Hong and Lim, 2006) and the Yonsei University planetary boundary layer scheme (Noh *et al*., 2001) are used in all domains, while the Kain–Fritsch cumulus parameterization scheme (Kain, 2004) is used only in d01 and d02. The simulation is initiated at 0000 UTC, and runs for 60 hr, a period that includes (a) the entire moving-out stage of the convective system originated from the TP and (b) the formation stage of the SWV. More-detailed model configurations and the design of the semi-idealized simulation can be found in Fu *et al*. (2019).

2.2 | Vorticity-budget equation

As the Green's theorem indicates, the surface integral of vorticity over a region equals the velocity circulation along its boundary line (i.e., the velocity circulation). This implies that if vorticity of the air particles that form a vortex enhances, the intensity of the vortex (reflected by the velocity circulation) will also increase. Therefore, the vorticity budget can effectively reflect the variation of a vortex. In this study, the Lagrangian vorticity-budget equation (Kirk, 2003) is used.

$$\frac{\mathrm{d}\varsigma}{\mathrm{d}t} = \mathbf{k}\cdot\left(\frac{\partial \mathbf{V}_h}{\partial p}\times\nabla_h\omega\right) - \beta v - (\varsigma + f)\nabla_h\cdot\mathbf{V}_h + RES, \quad (1)$$

TIL BTE STR

where ζ is the relative vorticity, $\frac{\mathrm{d}\cdot}{\mathrm{d}t} = \frac{\partial\cdot}{\partial t} + \mathbf{V}_h\cdot\nabla_h(\cdot) + \omega\frac{\partial\cdot}{\partial p}$, $\mathbf{k}$ is the unit vector pointing to the

zenith, $V_h = u\mathbf{i} + v\mathbf{j}$ is the horizontal wind vector, $\nabla_h = \frac{\partial}{\partial x}\mathbf{i} + \frac{\partial}{\partial y}\mathbf{j}$ is the horizontal gradient operator; f is the Coriolis parameter, p is the pressure $\omega = dp/dt$ and $\beta = \partial f/\partial y$. The terms TIL, BTE and STR denote the tilting, β effect and stretching, respectively. *RES* is the residual effect due mainly to friction and subgrid processes, which is not analyzed in the present study. Similar to Wang and Tan (2014), TIL, BTE and STR are calculated on the model grids (we use the output from d03) and then interpolated to the parcel locations along their trajectories.

2.3 | Parameters of a SWV

The definition of a SWV used in this study is as documented in Fu *et al*. (2015): a SWV is determined when a lower-tropospheric closed center at the stream field coupled with a remarkable positive vorticity center appears around the SCB (26–34°N, 103–110°E). The outline which is calculated by using the method developed by Rudeva and Gulev (2007) is used as the spatial range of a SWV. The period between the first and last detection of a same SWV is defined as its life span.

3 | OVERVIEW OF EVENT

The semi-idealized simulation reproduced the salient features of the eight events used in composite, particularly (a) the evolution of the eastward-moving convective system that originated over the TP, (b) the SWV formation around the SCB and (c) the precipitation in the downstream regions (Fu *et al*., 2019). Therefore, it is reasonable to take the simulation results as being representative of this type of SWV formation. As shown in Figure 1, during the formation stage of the SWV (from no vortex to SWV formation), a 200-hPa upper-level jet maintains intensity north of the TP. The SCB is located approximately in the right-hand side of the exit region of this upper-level jet, meaning that ascending motions will be suppressed by the secondary circulation associated with the jet (Holton, 2004). This could be why convective activities are weak around the SCB before $t = 33$ hr. In

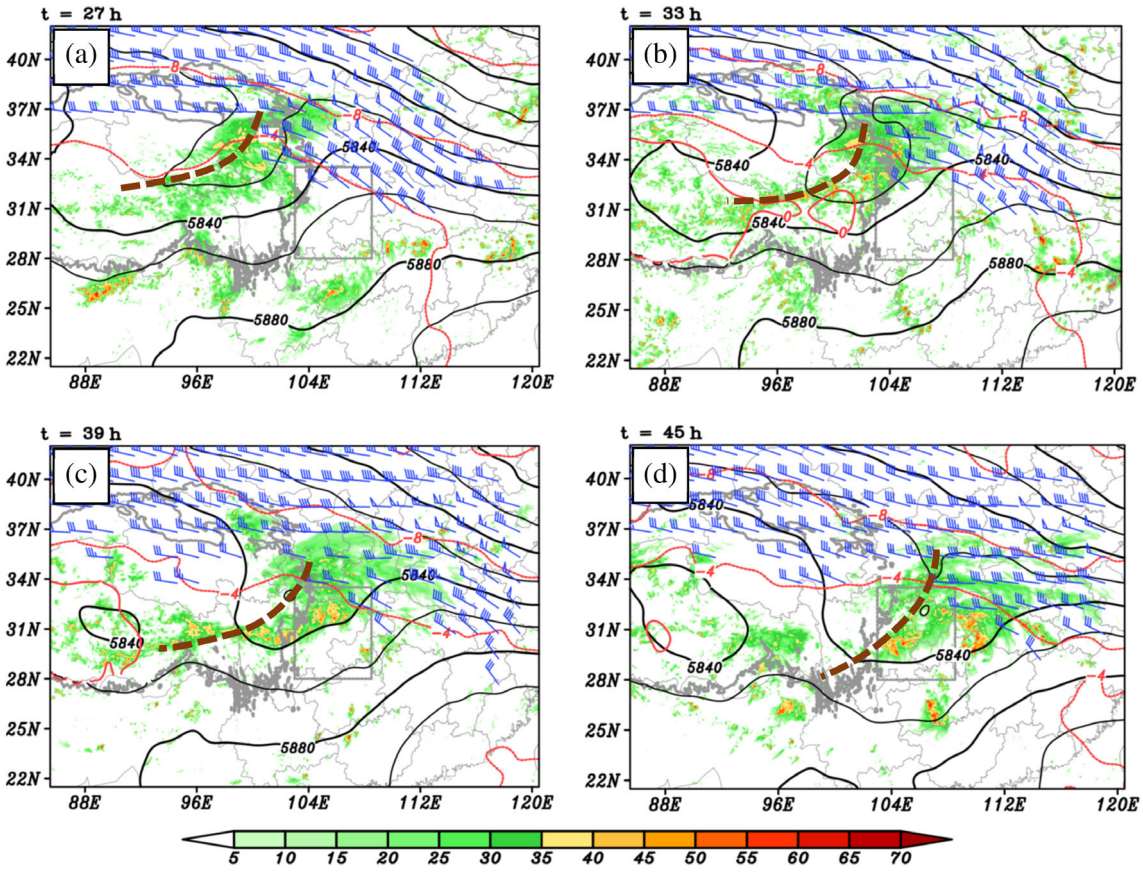

FIGURE 1 Composite reflectivity (shading, units: dBZ), 500-hPa geopotential height (black solid, units: gpm), 500-hPa temperature (red lines, units: °C) and 200-hPa wind with speed above 30 m/s (a full bar is 10 m/s), where the brown dashed lines mark the trough lines and the thick grey lines show the terrain above 3,000 m

the middle troposphere, a shortwave trough moves eastward from the TP, and an intense eastward-propagating convective system is located mainly within the central region of this trough. The shortwave trough and convective system are located mainly over the TP before $t = 33$ hr, whereupon they both begin to move out from the TP. As the trough does so, its intensity reduces (as the geopotential height shows) and the part of the convective system west of the trough line also weakens. Ahead of this shortwave trough, there is cyclonic-vorticity advection (not shown) and weak warm advection (corresponding to the sparse isotherms), both of which contribute to promoting ascending motions around the SCB (Holton, 2004). As the shortwave trough moves out from the TP (from $t = 39$ to 45 hr), convective activities around the SCB are enhanced considerably (Figure 1c, d). This is conducive to SWV formation through enhancing convergence and reducing pressure in the lower troposphere (Markowski and Richardson, 2010).

In the present study, the target SWV forms at $t = 45$ hr (i.e., the model has run for 45 hr) (Figure 2f), and lasts for the remaining 15 hr (the simulation is terminated at $t = 60$ hr). This is consistent with the SWVs that are used for composite, as all of them last for above 18 hr. From Figure 2f, the radius of the SWV is approximately 250 km, which is consistent with the SWVs' radii

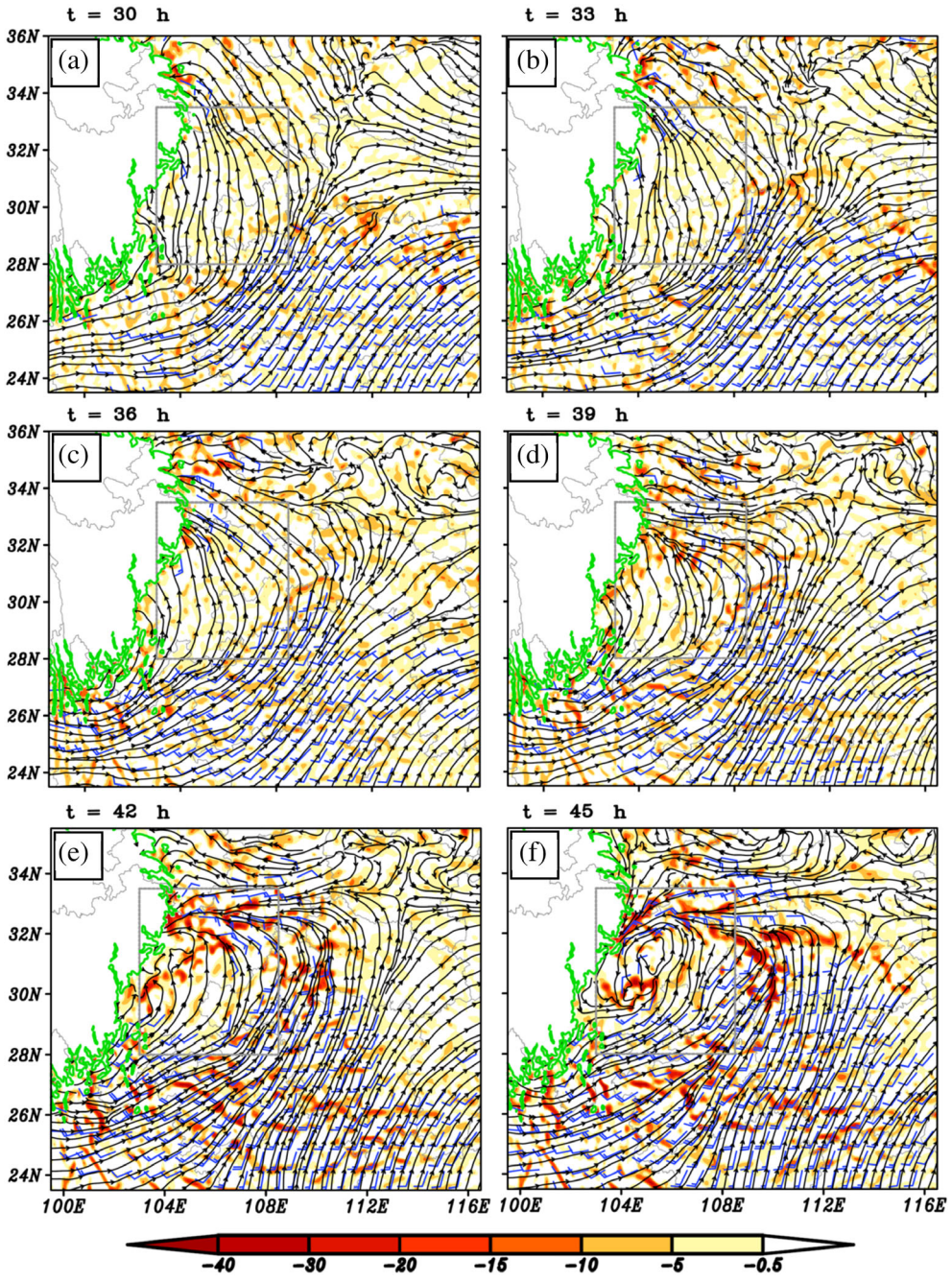

FIGURE 2 Stream field, divergence (shading, units: 10^{-5} s^{-1}) and wind with speed above 8 m/s (a full bar is 8 m/s) at 700 hPa, where the green lines outline terrain above 3,000 m and the grey box shows the key region of the southwest vortex (SWV)

in the eight events used for composite (not shown). Moreover, the distances between the center of the simulated SWV and the centers of SWVs that are used for composite are 20–70 km, which means the simulated SWV has similar locations to those SWVs used for composite. To focus on SWV formation, we define the 5.5° × 5.5° grey dashed box shown in Figure 2 as the key region. This covers the main body of the SWV and is insensitive to being changed by relatively small amounts (±0.5° to each boundary line). Before the shortwave trough and convective system move out from the TP, any ascending motion (Figure 1a, b), convergence (Figure 2a, b) and cyclonic vorticity (not shown) within the key region are relatively weak. A low-level jet appears southeast of the key region (Figure 2a, b), with strong convergence occurring mainly around its northern terminus. As the shortwave trough moves out from the TP, the convergence in the northern section of the SWV's key region intensifies rapidly (Figure 2c–f). Moreover, the low-level jet extends northward with time and enters the key region by t = 42 hr (Figure 2e, f), thereby enhancing the convergence around the southern boundary of the key region. This rapid enhancement of convergence helps to intensify the convective activities (through positive feedback between the ascending motion and the convergence) and the production of cyclonic vorticity (through the stretching effect) around the key region, both of which contribute to the SWV formation.

4 | ALONG-TRACK VORTICITY BUDGET FOR SWV FORMATION

4.1 | Overview

To answer the two scientific questions raised in the introduction, we conduct a backward tracking analysis [from t = 45 hr (SWV formation) to 0 hr] on the air particles that form the SWV based on a 15-min output of the WRF run. Air particles within the key region of the SWV (5.5° × 5.5°) are represented by 144 points with a constant longitude/latitude interval of 0.5° (Figure 3). Because 700 hPa is the central level of the SWV (Fu *et al.*, 2015), the backward tracking is initiated at 700 hPa using the aforementioned 144 points, based on the HYSPLIT model (Stein *et al.*, 2015). Figure 3 shows the tracks of these points, where 11 points in the northwestern section of the key region are missing because 700 hPa is under the terrain at these locations. Among the remaining 133 tracks, 60.1% come from levels lower than 700 hPa (>725 hPa) (green marks in Figure 4), 34.6%

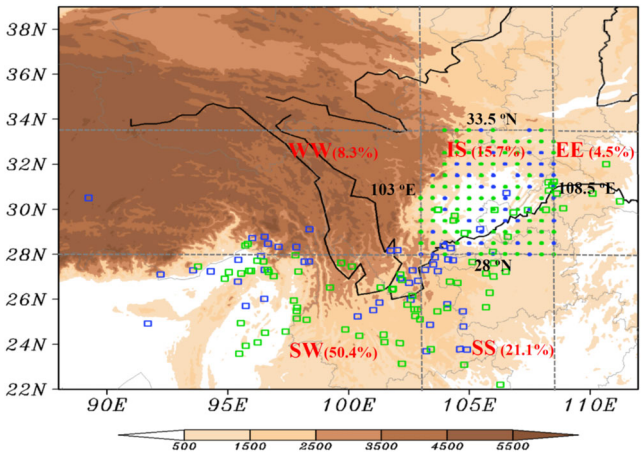

FIGURE 4 Initial (small open rectangles) and ending locations (small closed circles) of the 133 trajectories related to southwest vortex (SWV) formation; green/blue means the air particles originate from the lower levels/upper levels (LLs/ULs), grey dashed lines show the region divisions according to the key region of the SWV and corresponding contributions to the total number of trajectories (units: %)

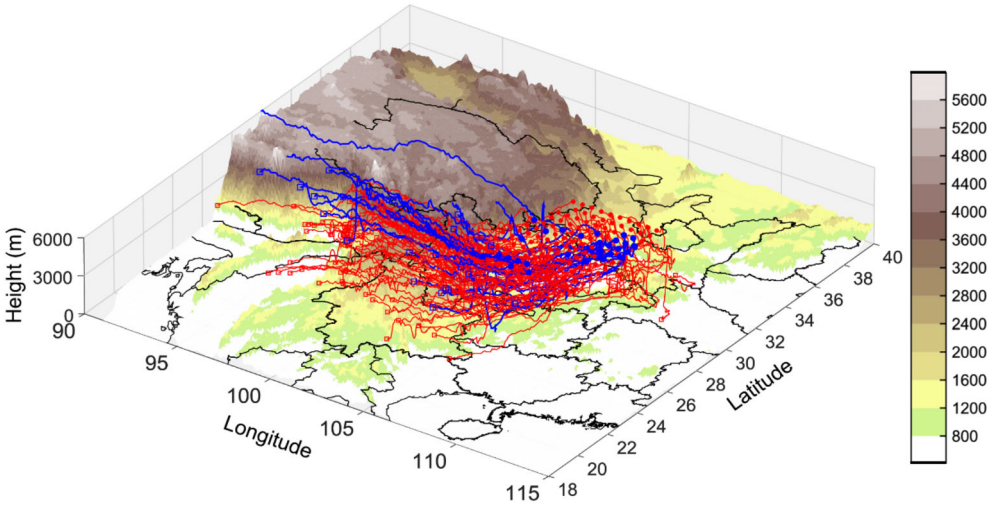

FIGURE 3 Three-dimensional illustration of backward trajectories of 700-hPa air particles around key area of the southwest vortex (SWV); closed circles mark locations of air particles at t = 45 hr and open rectangles mark locations at t = 0 hr. If an air particle is located above 5,000 m at any time from t = 0 to 45 hr, its trajectory is highlighted in blue, otherwise it is red. The colored surface is the terrain (units: m)

TABLE 1 Number contribution (NC) in all 133 tracks, contribution in initial ($t = 0$ hr) vorticity (CIV) of the 133 tracks and contribution in ending ($t = 45$ hr) vorticity (CEV) of the 133 tracks of different areas [western (WW), southwestern (SW), southern (SS), eastern (EE) and inside (IS) area] and levels [lower levels (LLs) and upper levels (ULs)] (units: %)

Contributions	EE		SS		SW		WW		IS	
	LLs	ULs	LLs	ULs	LLs	ULs	LLs	ULs	LLs	ULs
NC (94.7)	4.5	0.0	10.5	9.8	33.1	15.0	1.5	6.8	10.5	3.0
CIV (92.6)	0.2	0.0	49.9	19.5	24.1	11.3	−0.2	−12.6	2.6	−2.2
CEV (106.3)	−8.8	0.0	0.5	19.4	67.7	11.2	1.8	14.8	5.0	−5.3

come from levels higher than 700 hPa (<675 hPa) (blue marks in Figure 4) and only 5.3% come from levels around 700 hPa (725–675 hPa). For convenience, levels above 675 hPa are defined as the upper levels (ULs) and levels below 725 hPa are defined as the lower levels (LLs). As given in Table 1, the air particles (that form the SWV) coming from LLs account for approximately 76.6% and 66.2% of the total cyclonic vorticity associated with the SWV at $t = 0$ and 45 hr, respectively. This means that air particles originating from LLs are more important for SWV formation than are those from ULs and levels around the SWV.

Based on the longitudes and latitudes of the key region, nine areas are defined as shown in Figure 4. However, only the western (WW), southwestern (SW), southern (SS), eastern (EE) and inside (IS) areas act as sources for the air particles that form the SWV. Of these, IS accounts for only approximately 15.7% of the total air particles, which means that SWV formation is determined mainly by processes outside the key region. Overall, SW and SS are the two most-important air-particle sources for SWV formation, accounting for 50.4% and 21.1%, respectively. WW and EE also serve as air-particle sources for the SWV, but they make only small contributions. The air particles within these two regions show remarkably different behaviors: they mainly descend within WW but primarily ascend within EE (not shown).

4.2 | Vorticity budget

According to the contributions to the total cyclonic vorticity of the SWV when it forms ($t = 45$ hr), the SW LLs and the SS, WW and SW ULs are the top four air-particle sources. The air particles originating from these four sources account for approximately 64.7% of the total air-particle number, approximately 42.3% of the total initial cyclonic vorticity but up to approximately 113.1% of the total cyclonic vorticity of the SWV at $t = 45$ hr. The most rapid cyclonic-vorticity enhancement is due to these air particles. From $t = 0$ to 45 hr, the average cyclonic vorticity associated with these tracking air particles increases by approximately 3,020.0% (i.e., the ratio between the cyclonic vorticity increase from the start time to a given time and the cyclonic vorticity at the start time), which provides the necessary conditions for SWV formation. During stages I (0–15 hr), II (15–30 hr) and III (30–45 hr), the respective rates of cyclonic-vorticity variation associated with the air particles originating from the top four sources are approximately 580.0%, −13.2% and 428.8%. This means that the cyclonic vorticity of the tracking air particles does not always increase but rather it exhibits different features in different stages.

The air particles originating from the SW LLs occupy approximately 33.1% of the total air-particle number and account for approximately 24.1% and 67.7% of the total cyclonic vorticity at $t = 0$ and 45 hr, respectively (Table 1). As shown in Figure 5a–c, these air particles generally ascend in stages I and II with increasing potential temperature (latent heating) and decreasing specific humidity, which means that precipitation appears within the air particles. The vorticity budget shows that the cyclonic vorticity associated with these air particles generally decreases in stage I mainly because of divergence-related STR, whereas it increases in stage II mainly because of TIL. The most rapid increase of cyclonic vorticity appears in stage III, and its dominant factor is again TIL. As shown in Figure 5a–c, the tracking air particles generally experience precipitation evaporation in stage III because the potential temperature decreases (evaporative cooling) but the specific humidity increases. Overall, from $t = 0$ to 45 hr, the cyclonic vorticity of these air particles increases mainly because of TIL (its contribution is approximately 123.2%), whereas STR mainly acts conversely. The ascent and latent heating (mainly in stages I and II) of the tracking air particles contribute to the divergence associated with them. This is an important reason for why STR generally has negative effects upon the cyclonic-vorticity increase.

Overall, the air particles originating from the SS, WW and SW ULs account for approximately 31.6% of the total air-particle number and approximately 18.2% and 45.4% of the total cyclonic vorticity associated with the SWV at $t = 0$ and 45 hr, respectively (Table 1). Air particles

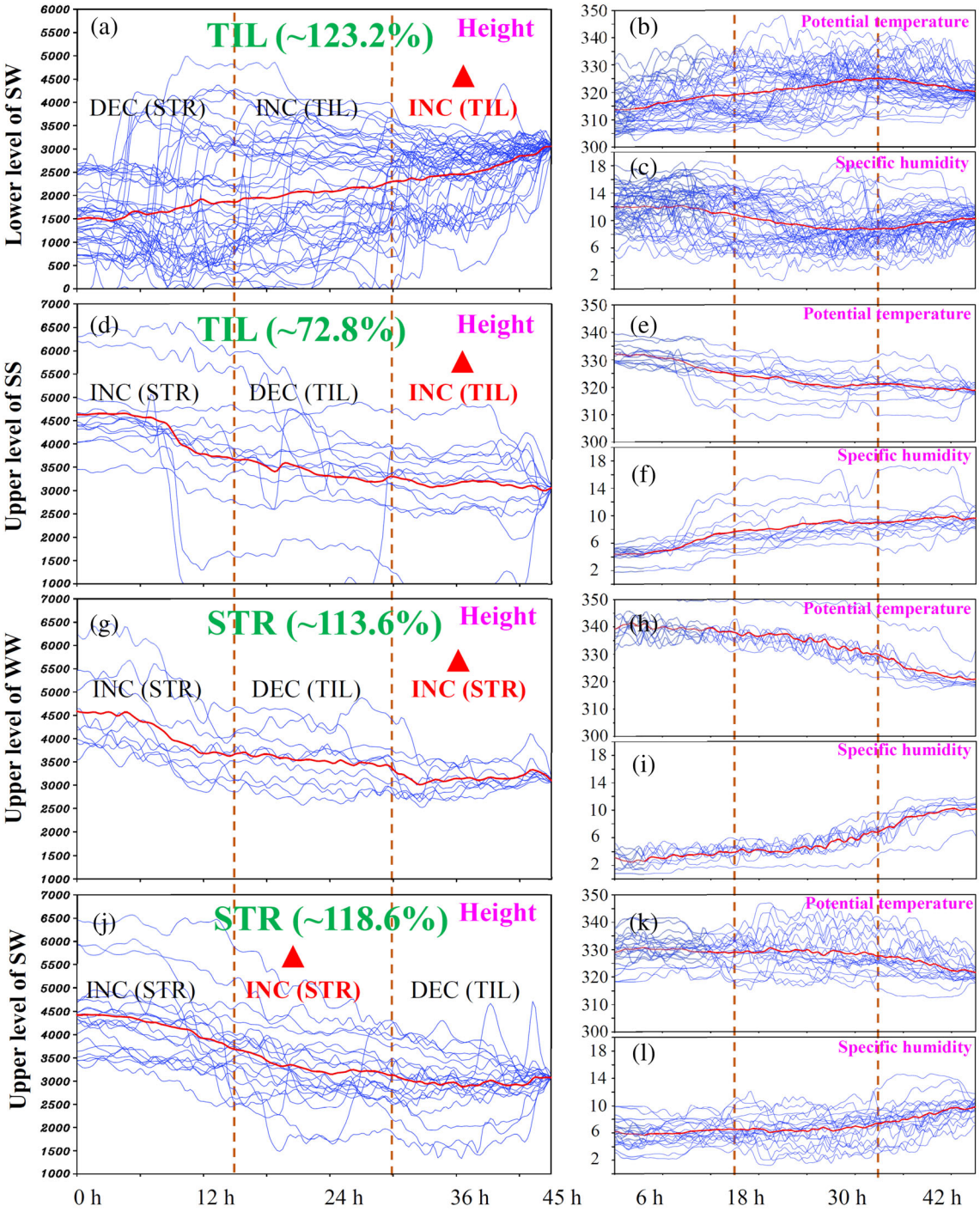

FIGURE 5 (a) Height (units: m), (b) potential temperature (units: K) and (c) specific humidity (g/kg) of tracking air particles from SW LLs (thin blue lines), along with their corresponding averaged states (thick red lines). In (a), the mean trends of the cyclonic vorticity associated with the tracking air particles in stages I–III are marked, with the dominant factors in parentheses. The dominant factor for the cyclonic-vorticity increase from $t = 0$ to 45 hr is shown in large green characters, with its contribution illustrated in parentheses. Panels (d–f) are as (a–c) but for the air particles from the SS ULs. Panels (g–i) are as (a–c) but for the air particles from the WW ULs. Panels (j–l) are as (a–c) but for the air particles from the SW ULs. DEC, decreasing cyclonic vorticity; INC, increasing cyclonic vorticity; LLs, lower levels; SS, southern; SW, southwestern; ULs, upper levels; WW, western

originating from these three sources generally descend with decreasing potential temperature and increasing specific humidity (Figure 5d–l), which means that precipitation evaporation occurs. This contributes to the convergence associated with these tracking air particles. In stage I, the cyclonic vorticity of the air particles

originating from these three sources increases mainly because of convergence-related horizontal shrinking (i.e., STR) (Figure 5d, g and j). In stage II, air particles originating from the SS and WW ULs mainly decrease in cyclonic vorticity because of tilting (i.e., TIL) (Figure 5d, g). By contrast, the most rapid cyclonic-vorticity increase associated with air particles originating from the SW ULs appears in stage II (Figure 5j), mainly because of convergence-related shrinking. The most rapid cyclonic-vorticity increase associated with air particles originating from the SS and WW ULs appears in stage III because of tilting and shrinking, respectively. By contrast, for the air particles originating from the SW ULs, their cyclonic vorticity generally decreases because of tilting. Overall, the convergence-related horizontal shrinking (i.e., STR) is the governing factor for the cyclonic-vorticity increase associated with the air particles originating from the SW and WW ULs, whereas tilting mainly acts conversely (Figure 5g, j). For the air particles originating from the SS ULs, tilting is dominant and convergence-related shrinking is also favorable (Figure 5d).

5 | CONCLUSIONS

Based on a composite semi-idealized simulation, this study focused on a type of heavy-rain-producing mesoscale-vortex formation (i.e., SWV formation) that is influenced by the eastward-propagating convective systems that originate over the TP. After confirming that the simulation reproduced the key features of this type of event, a trajectory analysis was conducted and an along-track vorticity budget was established for the simulated SWV. It was found that most of the air particles that formed the SWV came from five regions, namely WW, SW, SS, EE and IS. Overall, those air particles originated mainly from outside the key region (approximately 84.3%) rather than inside it, and they generally came from levels above and below 700 hPa (approximately 94.7%) rather than around the central level of the vortex. According to the contributions to SWV formation, the top four sources were determined as the SW LLs and the SS, WW and SW ULs. Those air particles were associated with rapid cyclonic-vorticity increase. However, the cyclonic vorticity did not increase persistently before SWV formation but rather exhibited different features in different stages. Generally, the most rapid cyclonic-vorticity enhancement tended to appear in stage III (excluding the air particles originating from the SW ULs).

The largest contribution to SWV formation (~67.7%) was made by air particles originating from the SW LLs. Overall, those air particles were associated with ascent and precipitation-related latent heating. Those features contributed to the divergence associated with those particles, which in turn rendered a negative STR (i.e., stretching) (with a contribution of approximately −23.2%). By contrast, tilting served as the dominant factor (approximately 123.2%) for the increase of cyclonic vorticity associated with those air particles. Overall, the air particles originating from the SS, WW and SW ULs contributed approximately 45.4% to SWV formation. Air particles originating from those three sources generally descended and experienced precipitation evaporation, both of which favor the convergence associated with those particles. Consequently, the convergence-related horizontal shrinking was the main contribution to the cyclonic-vorticity production associated with those particles, particularly for those originating from the SW and WW ULs, where STR acted as the dominant factor (whereas tilting acted conversely). For the air particles originating from the SS ULs, tilting dominated their cyclonic-vorticity increase (approximately 72.8%) and shrinking was also favorable.

As the output of a semi-idealized simulation may overestimate the impact of the large-scale circulation on the formation of SWV, in the future, each of the eight events used in the composite of this study will be investigated in detail and compared with the results derived from the semi-idealized simulation. This will enhance the understanding of this type of event.

ACKNOWLEDGEMENTS

The authors thank the National Centers for Environmental Prediction (NCEP) and the China Meteorological Administration for providing the data. This research was supported by the National Key R&D Program of China (grant no. 2018YFC0809400), the National Natural Science Foundation of China (grant nos. 41775046 and 91637211), and the Youth Innovation Promotion Association, Chinese Academy of Sciences.

DATA AVAILABILITY STATEMENT

[using OPS]Authors pay via card etc. ToC heading: Research Articles

ORCID

Shen-Ming Fu https://orcid.org/0000-0001-9670-0607
Yuan-Chun Zhang https://orcid.org/0000-0003-3038-9320

REFERENCES

Chen, Z.M., Xu, M.L., Min, W.B. and Miu, Q. (2003) Relationship between abnormal activities of southwest vortex and heavy rain the upper reach of Yangtze River during summer of 1998. *Plateau Meteorology*, 22, 162–167.

Fu, S.M., Sun, J.H., Zhao, S.X. and Li, W.L. (2011) The energy budget of a southwest vortex with heavy rainfall over South China. *Advances in Atmospheric Sciences*, 28(3), 709–724.

Fu, S.M., Zhang, J.P., Sun, J.H. and Shen, X.Y. (2014) A fourteen-year climatology of the southwest vortex in summer. *Atmospheric and Oceanic Science Letters*, 7, 510–514.

Fu, S.M., Li, W.L., Sun, J.H., Zhang, J.P. and Zhang, Y.C. (2015) Universal evolution mechanisms and energy conversion characteristics of long-lived mesoscale vortices over the Sichuan Basin. *Atmospheric Science Letters*, 16, 127–134.

Fu, S.M., Mai, Z., Sun, J.H., Li, W.L., Ding, Y. and Wang, Y.Q. (2019) Impacts of convective activity over the Tibetan Plateau on plateau vortex, southwest vortex, and downstream precipitation. *Journal of Atmospheric Sciences*, 76, 3803–3830. https://doi.org/10.1175/JAS-D-18-0331.1.

Holton, J.R. (2004) *An Introduction to Dynamic Meteorology*. San Diego, CA: Academic Press.

Hong, S.Y. and Lim, J.O. (2006) The WRF single-moment microphysics scheme (WSM6). *Journal of Korean Meteorological Society*, 42, 129–151.

Kain, J.S. (2004) The Kain–Fritsch convective parameterization: An update. *Journal of Applied Meteorology*, 43, 170–181.

Kirk, J.R. (2003) Comparing the dynamical development of two mesoscale convective vortices. *Monthly Weather Review*, 131, 862–890.

Kuo, Y., Cheng, L. and Bao, J. (1988) Numerical simulation of the 1981 Sichuan Flood. Part I: Evolution of a mesoscale southwest vortex. *Monthly Weather Review*, 116, 2481–2504.

Li, L., Zhang, R.H. and Wen, M. (2017) Genesis of southwest vortices and its relation to Tibetan Plateau vortices. *Quarterly Journal of the Royal Meteorological Society*, 143, 2556–2566.

Lu, J.H. (1986) *Generality of the Southwest Vortex*. Beijing: China Meteorological Press.

Markowski, P. and Richardson, Y. (2010) *Mesoscale Meteorology in Midlatitudes*. Hoboken, NJ: Wiley-Blackwell.

Ni, C.C., Li, G.P. and Xiong, X.Z. (2017) Analysis of a vortex precipitation event over southwest China using AIRS and in situ measurements. *Advances in Atmospheric Sciences*, 34, 559–570.

Noh, Y., Cheon, W.G. and Raasch, S. (2001) *The Improvement of the K-Profile Model for the PBL Using LES*. Seoul: Preprints of the International Workshop of Next Generation NWP Model, pp. 65–66.

Rudeva, I. and Gulev, S.K. (2007) Climatology of cyclone size characteristics and their changes during the cyclone life cycle. *Monthly Weather Review*, 135, 2568–2587.

Saha, S., Moorthi, S., Pan, H.L., Wu, X.G., Wang, J.D., Nadiga, S., Tripp, P., Kistler, R., Woollen, J., Behringer, D., Liu, H.X., Stokes, D., Grumbine, R., Gayno, G., Wang, J., Hou, Y.T., Chuang, H.Y., Juang, H.M.H., Sela, J., Iredell, M., Treadon, R., Kleist, D., Delst, P.V., Keyser, D., Derber, J., Michael, E., Meng, J., Wei, H.L., Yang, R.Q., Lord, S., Dool, H.V.D., Kumar, A., Wang, W.Q., Long, C., Chelliah, M., Xue, Y., Huang, B.Y., Schemm, J.K., Ebisuzaki, W., Lin, R., Xie, P.P., Chen, M.Y., Zhou, S.T., Higgins, W., Zou, C.Z., Liu, Q.H., Chen, Y., Han, Y., Cucurull, L., Reynolds, R.W., Rutledge, G. and Goldberg, M. (2010) The NCEP climate forecast system reanalysis. *Bulletin of the American Meteorological Society*, 91, 1015–1057.

Skamarock, W.C. Klemp, J.B., Dudhia, J., Gill, D.O., Barker, D.M., Duda, M.G., Huang, X.Y., Wang, W., and Powers, J.G. (2008) A description of the Advanced Research WRF version 3. NCAR Tech. Note CAR/TN-475+STR, pp. 113.

Stein, A.F., Draxler, R.R., Rolph, G.D., Stunder, B.J.B., Cohen, M.D. and Ngan, F. (2015) NOAA'S HYSPLIT atmospheric transport and dispersion modeling system. *Bulletin of the American Meteorological Society*, 96, 2059–2077.

Wang, Q.W. and Tan, Z.M. (2014) Multi-scale topographic control of southwest vortex formation in Tibetan Plateau region in an idealized simulation. *Journal of Geophysical Research: Atmospheres*, 119, 11543–11561.

Zhang, J.P., Fu, S.M., Sun, J.H., Shen, X.Y. and Zhang, Y.C. (2015) A statistical and compositional study on the two types of mesoscale vortices over the Yangtze River basin. *Climatic and Environmental Research*, 20, 319–336.

Zhao, S.X. and Fu, S.M. (2007) An analysis on the southwest vortex and its environment fields during heavy rainfall in eastern Sichuan Province and Chongqing in September 2004. *Chinese Journal of Atmospheric Sciences*, 31, 1059–1075.

Zhao, P. and Hu, C.Q. (1992) Numerical simulation and diagnosis of the formation process of SW vortex. *Chinese Journal of Atmospheric Sciences*, 16, 177–184.

Zhao, S.X., Tao, Z.Y., Sun, J.H. and Bei, N.F. (2004) *Study on Mechanism of Formation and Development of Heavy Rainfalls on Meiyu Front in Yangtze River*. Beijing: China Meteorological Press.

Zhong, R., Zhong, L.H., Hua, L.J. and Feng, S.D. (2014) A climatology of the southwest vortex during 1979–2008. *Atmospheric and Oceanic Science Letters*, 7, 577–583.

How to cite this article: Feng S-L, Jin S-L, Fu S-M, Sun J-H, Zhang Y-C. Formation of a kind of heavy-precipitation-producing mesoscale vortex around the Sichuan Basin: An along-track vorticity budget analysis. *Atmos Sci Lett*. 2020;21:e949. https://doi.org/10.1002/asl.949